

# Agile Reinforcement Learning through Separable Neural Architecture

Rajib Mostakim<sup>1</sup> Reza T. Batley<sup>2</sup> Sourav Saha<sup>2</sup>

## Abstract

Deep reinforcement learning (RL) is increasingly deployed in resource-constrained environments, yet the go-to function approximators - multi-layer perceptrons (MLPs) - are often parameter-inefficient due to an imperfect inductive bias for the smooth structure of many value functions. This mismatch can also hinder sample efficiency and slow policy learning in this capacity-limited regime. Although model compression techniques exist, they operate post-hoc and do not improve learning efficiency. Recent spline-based separable architectures - such as Kolmogorov-Arnold Networks (KANs) - have been shown to offer parameter efficiency but are widely reported to exhibit significant computational overhead, especially at scale.

In seeking to address these limitations, this work introduces SPAN (**SP**line-based **A**daptive **N**euro**Ps**), a novel function approximation approach to RL. SPAN adapts the low rank KHRONOS framework by integrating a learnable preprocessing layer with a separable tensor product B-spline basis. SPAN is evaluated across discrete (PPO) and high-dimensional continuous (SAC) control tasks, as well as offline settings (Minari/D4RL). Empirical results demonstrate that SPAN achieves a **30-50% improvement in sample efficiency** and **1.3-9 times higher success rates** across benchmarks compared to MLP baselines. Furthermore, SPAN demonstrates superior anytime performance and robustness to hyperparameter variations, suggesting it as a viable, high performance alternative for learning intrinsically efficient policies in resource-limited settings.

<sup>1</sup> Department of Mechanical Engineering, Bangladesh University of Engineering and Technology, Dhaka, Bangladesh <sup>2</sup> Kevin T. Crofton Department of Aerospace and Ocean Engineering, Virginia Polytechnic Institute and State University, Blacksburg, VA, USA . Correspondence to: Sourav Saha <sourav.saha@vt.edu>.

## 1. Introduction

Deep reinforcement learning has achieved remarkable success across diverse domains including game playing (Mnih et al., 2015; Silver et al., 2017), robotic manipulation (Levine et al., 2016; Kalashnikov et al., 2018), autonomous navigation (Kahn et al., 2017; Tai et al., 2017), and industrial optimization (Mao et al., 2016). These achievements fundamentally rely on neural function approximation to represent policies and value functions. The dominant approach employs multilayer perceptrons (MLPs) with ReLU activations, chosen for their universal approximation properties (Hornik et al., 1989).

However, deploying RL in real-world applications faces critical resource constraints. Physical systems incur real costs per interaction and have limited samples (Dulac-Arnold et al., 2019), edge devices impose strict memory budgets (Li et al., 2020), and production environments frequently face training interruptions (Zilberstein, 1996). Standard MLPs, which typically require hundreds of hidden units to represent smooth value functions, struggle under these constraints due to high sample complexity (Kakade, 2003) and uniform capacity distribution.

Addressing these limitations requires moving beyond MLPs toward architectures that can learn complex control policies with high sample efficiency under strict resource constraints without sacrificing training stability. This article introduces SPAN (**SP**line-based **A**daptive **N**euro**Ps**), a parameter efficient architecture tailored for resource-constrained RL. SPAN extends the KHRONOS framework (Batley & Saha, 2025) designed for scientific computing by integrating a learnable preprocessing layer. The central insight driving this approach is that RL value functions and policies exhibit local smoothness; small changes in state typically produce small changes in value or action, making them naturally suited to spline-based approximation. Unlike MLPs, which distribute capacity uniformly, B-splines concentrate representational power through local support, providing an inductive bias directly aligned with the structure of control problems. By leveraging a rank  $M$  tensor decomposition, SPAN overcomes the curse of dimensionality inherent in traditional grid-based splines. This reduces parameter complexity from exponential to linear with respect to input dimension, enabling scalability to high-dimensional tasks.

SPAN leverages the local support of B-splines to achieve high parameter efficiency compared to global MLPs, while offering continuous derivatives that stabilize policy gradients. The contributions of this work are twofold. First, SPAN is adapted for reinforcement learning, creating a parameter efficient architecture with inherent smoothness guarantees. Second, SPAN is empirically validated across Classic Control and MuJoCo from the gymnasium (Towers et al., 2024) and D4RL datasets from the Minari datasets (Younis et al., 2024) under strict parameter constraints, demonstrating a 30% to 50% improvement in sample efficiency and 1.3 to 9 times higher success rates. Collectively, these results demonstrate that SPAN significantly improves both sample and parameter efficiency in resource-constrained settings, providing a practical, high performance alternative to MLPs when deployment constraints limit model capacity or training budgets.

The remainder of this article is organized as follows. Section 2 reviews prior work in RL and the recent emergence of spline-based architectures in scientific computing. Section 3 establishes RL preliminaries. Section 4 details the SPAN architecture. Section 5 presents empirical evaluations across online and offline control benchmarks. Section 6 analyzes the structural inductive bias and discusses current limitations, followed by concluding remarks in Section 7.

## 2. Related Work

Modern deep RL predominantly employs multilayer perceptrons (MLPs) for policy and value function approximation (Mnih et al., 2015; Lillicrap et al., 2019; Schulman et al., 2017; Haarnoja et al., 2018). While justified by universal approximation guarantees (Hornik et al., 1989), standard MLPs typically require hundreds of hidden units to represent smooth control landscapes accurately. To improve optimization stability, prior research has explored activation functions such as Swish and GELU (Ramachandran et al., 2017; Hendrycks & Gimpel, 2023), as well as architectural stabilizers including layer normalization and residual connections (Ba et al., 2016; He et al., 2015). While these techniques improve optimization stability, they preserve the fully connected MLP structure with uniformly distributed capacity, which often leads to sample inefficiency in learning.

A substantial body of work focuses on reducing the size of neural networks via pruning (Han et al., 2016), quantization (Jacob et al., 2017), or knowledge distillation (Hinton et al., 2015). However, these techniques generally operate as *post hoc* optimization steps on over-parameterized models, primarily targeting inference latency rather than training efficiency. Similarly, factorized networks (Sainath et al., 2013) and tensor decompositions (Novikov et al., 2015) reduce parameter counts by imposing low rank structures on weight

matrices, but retain global connectivity. In contrast, SPAN targets *intrinsic learning efficiency*, reducing the number of environment interactions required to learn a performant policy directly under fixed, low capacity constraints, without expensive pre-training or compression phases. Overall, SPAN is a different function approximation paradigm that achieves parameter and sample efficiency intrinsically.

Recently, Kolmogorov Arnold Networks (KANs) (Liu et al., 2025) have emerged as a spline-based alternative to MLPs for reducing parameter counts while preserving expressive power. In offline reinforcement learning, KANs can match MLP performance with fewer parameters, but pure KAN architectures often underperform compared to hybrid KAN-MLP models and incur higher training costs (Guo et al., 2024). Similarly, KANs have been applied to online continuous control tasks (Kich et al., 2024), reporting comparable performance to MLPs with reduced memory usage. However, this study highlighted a significant computational bottleneck: the dense evaluation of B-splines on every network edge resulted in training times approximately nine times slower than standard MLPs. Furthermore, performance stability varied significantly across tasks, with KANs underperforming against baselines.

Parallel to KANs, the KHRONOS framework (Batley & Saha, 2025) introduced a separable tensor product B-splines architecture for scientific computing. The framework has been validated across diverse scientific domains, including multi-fidelity aerodynamic prediction (Sarker et al., 2026), inverse material design (Batley & Saha, 2026), fatigue life estimation and application in additive manufacturing (Mostakim et al., 2025; Park et al., 2025). However, while these works demonstrate the efficacy of the architecture for supervised regression, its application to the dynamic, sequential decision making challenges of Reinforcement Learning remains unexplored.

This work introduces SPAN to bridge this gap. Rather than using a raw KHRONOS architecture, SPAN incorporates a learnable preprocessing layer to project unstructured observations into a feature space suitable for tensor product operations. By coupling this adaptation, SPAN offers a function approximation paradigm inherently aligned with the local smoothness of control policies. Furthermore, this study provides a comprehensive evaluation specifically isolating sample efficiency and anytime performance metrics critical for deployment in resource-constrained settings rather than solely focusing on final asymptotic performance.

## 3. Theoretical Background

### 3.1. Reinforcement Learning Preliminaries

The standard reinforcement learning framework is formalized as a Markov Decision Process (MDP) defined by the

tuple  $(\mathcal{S}, \mathcal{A}, P, r, \gamma)$ , (Sutton & Barto, 2018) where  $\mathcal{S}$  is the state space,  $\mathcal{A}$  is the action space,  $P : \mathcal{S} \times \mathcal{A} \times \mathcal{S} \rightarrow [0, 1]$  is the transition probability function,  $r : \mathcal{S} \times \mathcal{A} \rightarrow \mathbb{R}$  is the reward function, and  $\gamma \in [0, 1)$  is the discount factor.

The agent’s behavior is determined by a policy  $\pi : \mathcal{S} \rightarrow \mathcal{P}(\mathcal{A})$ , which maps states to probability distributions over actions. The objective is to find a policy that maximizes the expected cumulative discounted reward (Sutton et al., 1999):

$$J(\pi) = \mathbb{E}_{\tau \sim \pi} \left[ \sum_{t=0}^{\infty} \gamma^t r(s_t, a_t) \right]$$

where  $\tau = (s_0, a_0, s_1, a_1, \dots)$  denotes a trajectory sampled by executing policy  $\pi$ .

Value-based and policy-based approaches differ in whether they learn an explicit value function ( $V^\pi(s)$ ), an action-value ( $Q^\pi(s, a)$ ), or a direct parametric policy ( $\pi_\theta(a|s)$ ). In continuous or large discrete state/action spaces, exact representation of value functions or policies is intractable. Modern deep reinforcement learning employs parameterized function approximators  $Q_\theta(s, a)$  and  $\pi_\phi(a|s)$  to represent these functions.

### 3.2. Reinforcement Learning Algorithms

**Soft Actor-Critic (SAC)** is an off-policy actor-critic algorithm for continuous control that optimizes a maximum entropy objective (Haarnoja et al., 2018; 2019). By explicitly encouraging stochasticity in the policy, SAC promotes effective exploration. The algorithm employs a stochastic policy, twin Q-functions to reduce overestimation bias, and slowly updated target networks for stable learning. Policy and value functions are learned jointly from off policy data, and the entropy temperature can be automatically adjusted to balance exploration and reward maximization.

**Proximal Policy Optimization (PPO)** is an on-policy policy gradient method that improves training stability by restricting the magnitude of policy updates (Schulman et al., 2017). PPO uses advantage estimates to guide policy improvement while preventing destructive updates through a clipped objective. In practice, advantages are commonly estimated using Generalized Advantage Estimation (GAE) (Schulman et al., 2018). PPO further incorporates a value function loss and an entropy bonus.

**Implicit Q-Learning (IQL)** is an offline reinforcement learning algorithm designed to avoid explicit behavior policy estimation (Kostrikov et al., 2021). IQL learns a Q-function via asymmetric value regression, encouraging conservatism by penalizing overestimation of unseen actions. Policy learning is performed by advantage weighted regression, where actions with higher estimated advantages are

assigned higher likelihood under the learned policy. This implicit constraint enables stable learning from fixed datasets without requiring importance sampling or explicit policy constraints, making IQL effective in offline and limited-data regimes.

## 4. Method: SPAN for Reinforcement Learning

### 4.1. Architectural Foundation

SPAN (SPline-based Adaptive Networks) builds upon tensor product B-spline architectures for function approximation. For completeness, the KHRONOS (Kernel-Expansion Hierarchy for Reduced-Order, Neural-Optimized Surrogates) formulation (Batley & Saha, 2025) is briefly reviewed before introducing SPAN’s RL-specific adaptations.

Given input  $\mathbf{x} \in [0, 1]^d$ , KHRONOS constructs  $M$  separable modes via per-dimension B-spline basis expansions followed by tensor products:

$$\mathcal{M}_j(\mathbf{x}) = \prod_{p=1}^d \sum_{i=1}^{N_p} w_{p,j,i} B_i^{(k)}(x_p)$$

where  $B_i^{(k)}$  are B-spline basis functions of degree  $k$ ,  $N_p$  is the number of basis functions per-dimension, and  $w_{p,j,i}$  are learnable weights. The final output combines all modes through a linear head:

$$f(\mathbf{x}) = \mathbf{W} \begin{bmatrix} \mathcal{M}_1(\mathbf{x}) \\ \vdots \\ \mathcal{M}_M(\mathbf{x}) \end{bmatrix} + \mathbf{b}$$

This separable structure reduces parameter complexity from  $\mathcal{O}(N^d)$  (full tensor grid) to  $\mathcal{O}(MdN)$  (linear in dimension).

### 4.2. SPAN

While KHRONOS operates on normalized inputs  $[0, 1]^d$ , RL environments yield observations with arbitrary ranges and distributions. SPAN addresses this through a preprocessing layer that normalizes inputs before B-spline evaluation. (Figure 1). A single fully-connected layer with sigmoid activation:

$$\mathbf{z} = \sigma(\mathbf{W}_{\text{pre}} \mathbf{s} + \mathbf{b}_{\text{pre}})$$

where  $\mathbf{s} \in \mathbb{R}^d$  is the environment observation,  $\mathbf{W}_{\text{pre}} \in \mathbb{R}^{d \times d}$ ,  $\mathbf{b}_{\text{pre}} \in \mathbb{R}^d$ , and  $\sigma(\cdot)$  is the elementwise sigmoid. This adds only  $d^2 + d$  parameters negligible compared to the KHRONOS core but provides three critical benefits: (1) projects arbitrary input ranges to  $[0, 1]^d$  where B-splines are well defined, (2) standardizes input scales across dimensions, and (3) enables feature recombination before nonlinear spline processing.

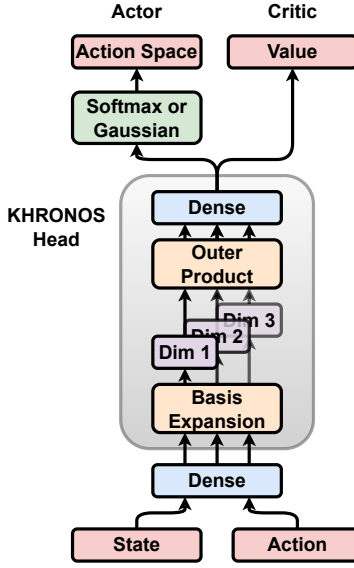


Figure 1. SPAN architecture for actor-critic reinforcement learning. Environment states, action or state-action pair pass through a preprocessing layer (Dense + Sigmoid) that normalizes inputs to  $[0, 1]^d$ . Per-dimension B-spline basis expansions generate univariate features, which are combined via tensor products (outer product) across dimensions to form  $M$  separable modes. A linear head produces task specific outputs: policy logits (with softmax) for discrete actions or Gaussian parameters (mean, std) for continuous actions. Both actor and critic use identical SPAN architectures with separate parameters.

The SPAN forward pass composes preprocessing and tensor product splines:

$$\text{SPAN}(\mathbf{s}; \Theta) = \mathbf{W} \begin{bmatrix} \mathcal{M}_1(\mathbf{z}) \\ \vdots \\ \mathcal{M}_M(\mathbf{z}) \end{bmatrix} + \mathbf{b}, \quad \mathbf{z} = \sigma(\mathbf{W}_{\text{pre}} \mathbf{s} + \mathbf{b}_{\text{pre}})$$

where  $\Theta = \{\mathbf{W}_{\text{pre}}, \mathbf{b}_{\text{pre}}, \{w_{p,j,i}\}, \mathbf{W}, \mathbf{b}\}$  contains all learnable parameters.

#### 4.3. Integration with Reinforcement Learning Algorithms

SPAN serves as a drop-in replacement for MLPs in standard actor-critic frameworks. We detail integration with SAC (continuous control) and PPO (discrete control).

##### 4.3.1. SOFT ACTOR-CRITIC (SAC)

**Actor (Gaussian Policy):** For continuous actions, SPAN outputs mean and log-standard-deviation:

$$[\mu_\theta(s); \log \sigma_\theta(s)] = \text{SPAN}_\theta^{\text{actor}}(s)$$

where  $\text{SPAN}_\theta^{\text{actor}} : \mathbb{R}^d \rightarrow \mathbb{R}^{2A}$  with  $A$  the action dimension. Actions are sampled via reparameterization  $a = \mu_\theta(s) + \sigma_\theta(s) \odot \epsilon$  with  $\epsilon \sim \mathcal{N}(0, I)$ , followed by tanh squashing for bounded action spaces.

**Twin Critics:** Each Q-function maps concatenated state-action pairs to scalar values:

$$Q_{\theta_i}(s, a) = \text{SPAN}_{\theta_i}^{\text{critic}}([s; a]), \quad i \in \{1, 2\}$$

where  $\text{SPAN}_{\theta_i}^{\text{critic}} : \mathbb{R}^{d+A} \rightarrow \mathbb{R}$ . The SAC training loop proceeds unchanged with SPAN as the function approximator.

##### 4.3.2. PROXIMAL POLICY OPTIMIZATION (PPO)

**Policy:** For discrete actions, SPAN outputs logits over  $A$  actions:

$$\pi_\theta(a|s) = \text{Categorical}(\text{softmax}(\text{SPAN}_\theta^{\text{actor}}(s)))$$

where  $\text{SPAN}_\theta^{\text{actor}} : \mathbb{R}^d \rightarrow \mathbb{R}^A$ .

**Value Function:** The critic estimates state values via  $\text{SPAN}_\phi^{\text{critic}} : \mathbb{R}^d \rightarrow \mathbb{R}$ :

$$V_\phi(s) = \text{SPAN}_\phi^{\text{critic}}(s)$$

GAE computation and PPO’s clipped objective remain identical to standard implementations.

##### 4.3.3. IMPLICIT Q-LEARNING (IQL)

IQL requires three distinct function approximators: a value function  $V(s)$ , a Q-function  $Q(s, a)$ , and a policy  $\pi(a|s)$ . SPAN replaces the MLP in all three roles:

$$V_\psi(s) = \text{SPAN}_\psi^{\text{value}}(s), \quad Q_\theta(s, a) = \text{SPAN}_\theta^{\text{critic}}([s; a])$$

$$\pi_\phi(a|s) = \mathcal{N}(\mu_\phi(s), \Sigma_\phi(s)) \quad \text{via} \quad \text{SPAN}_\phi^{\text{actor}}(s)$$

where inputs to the Q-network are concatenated state-action pairs  $[s; a]$ .

## 5. Experimental Setup and Results

SPAN is evaluated and compared with standard MLP baselines across diverse reinforcement learning domains to comprehensively assess performance and robustness. Experiments cover on-policy algorithm PPO for Classic Control tasks (CartPole, Acrobot) and a Box2D task (Lunar Lander), off-policy method SAC for continuous control MuJoCo tasks (Hopper, InvertedPendulum, HalfCheetah), and offline RL (IQL) for the Adroit Hand tasks. The performance of online RL is assessed through two complementary benchmarks: *sample efficiency* and *anytime performance* that directly address key practical constraints in real-world RL deployment. For offline RL, as online interaction is prohibited during training, the final performance result is reported.

**Sample Efficiency** is quantified as the number of environment interaction steps required for an agent to reach specific performance milestones, measured at 25%, 50%, 75%, 95%, and 100% of an expert-level score. The expert targets are defined as follows: for *Acrobot* and *LunarLander*, the official “solved” criteria from the Gymnasium documentation; for *CartPole* and *InvertedPendulum*, the theoretical maximum return imposed by the horizon limit; and for unbounded tasks like *Hopper* and *HalfCheetah*, scores indicative of a stable, high-velocity locomotion gait. To ensure robustness, “sustained solving” is implemented; this is defined as achieving the target return over 30 evaluation episodes for five consecutive evaluation intervals (occurring every 5,000 steps). This metric is particularly important in robotics and physical systems, where learning must often be performed directly on the real system using a limited number of samples, and each environment interaction may incur nontrivial costs such as mechanical wear or increased wall-clock time (Dulac-Arnold et al., 2019). Consequently, reducing the number of interactions required to achieve target performance can directly lower deployment and experimentation costs. Resource-constrained devices (mobile robots, IoT sensors, embedded systems) have strict memory budgets that limit model capacity. When parameter counts are fixed at hundreds or low thousands, sample efficiency becomes the primary axis for improvement, as simply scaling model size is not feasible. The high variance and sensitivity of deep reinforcement learning methods necessitate repeated experimentation and careful tuning (Henderson et al., 2019), making rapid iteration challenging. Methods that reduce the number of required environment interactions can thus facilitate faster prototyping and evaluation.

**Anytime Performance** is the agent performance at multiple checkpoints during training: 10% 25%, 50%, 75%, 95% and 100% of the total training budget steps. At each checkpoint, mean return with standard deviation is measured. This metric is crucial for production environments where training may be preempted due to strict time constraints, budget exhaustion, or resource contention in shared clusters. Anytime performance quantifies the quality of policies available at arbitrary stopping points, enabling practitioners to optimize the trade-off between performance and computational cost.

Together, sample efficiency and anytime performance provide a holistic measure of learning efficiency, capturing both the speed to reach target performance and the evolution of policy quality throughout training. Under real-world constraints such as limited interactions, or fixed model capacities, both metrics are critical. Sample efficiency results, including success rates and median steps to each threshold, are presented in this section alongside raw evaluation curves showing learning trajectories. Anytime performance results are provided in Appendix A. Training details, algorithm specific hyperparameters, and total training parameter counts

are reported in Appendix B. Complete ablation studies are reported in Appendix C and hardware Specifications are reported in Appendix D.

### 5.1. Online Reinforcement Learning Results

**Classic Control:** Two standard Gymnasium discrete control environments *CartPole* and *Acrobot* and one *Box2D* environment, *LunarLander*, are evaluated using PPO (Schulman et al., 2017). *CartPole* involves stabilizing a pole on a moving cart with a 4-dimensional state space and 2 discrete actions. *Acrobot* requires swinging a two-link underactuated pendulum to a target height, operating in a 6 dimensional state space with 3 actions. *LunarLander* tasks the agent with navigating a spacecraft to a designated landing pad using main and side thrusters, with an 8 dimensional state space and 4 actions. Figure 2 reports learning curves showing mean episodic return with  $\pm$  one standard deviation across 20 random seeds. Sample efficiency results are summarized in Table 1, while anytime performance is reported in Appendix A.

Across all Classic Control environments, SPAN consistently demonstrates faster learning and reduced variance compared to the MLP baseline. In *CartPole*, SPAN reaches 50% of expert performance in a median of 73k environment steps, compared to 86k for MLP, and achieves a 100% success rate versus 95% for MLP. At the 100% performance threshold, SPAN solves the task in 201k steps with a 95% success rate, whereas MLP requires 300k steps and achieves only 75% success.

*LunarLander* exhibits moderate but consistent improvements. SPAN reaches 50% expert performance in 283k steps, compared to 476k for MLP, corresponding to a 40% reduction in required interactions, with both methods achieving perfect success rates. At the 100% threshold, SPAN maintains a 90% success rate while solving in 618k steps, whereas MLP drops to a 60% success rate and requires 810k steps.

*Acrobot*, characterized by sparse rewards and negative returns, further highlights SPAN’s robustness. At the 50% threshold (corresponding to a score of -200), SPAN achieves a 95% success rate and solves the task in 105k steps, compared to MLP’s 65% success rate and 175k steps. This approximately 40% speedup persists at the 100% threshold, where SPAN maintains a 90% success rate while MLP again drops to 60%.

**MuJoCo Continuous Control:** SPAN is evaluated on three MuJoCo continuous control environments: *InvertedPendulum*, *Hopper*, and *HalfCheetah* using Soft Actor-Critic (SAC) (Haarnoja et al., 2018). *InvertedPendulum* requires balancing a single link pendulum in an upright position by applying continuous horizontal forces to a sliding cart.

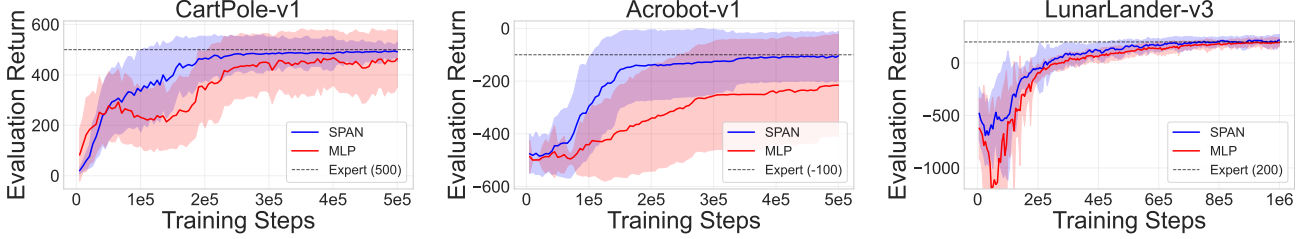


Figure 2. Reward curves for Classic Control and Box2D environments showing mean performance  $\pm$  1 standard deviation across 20 seeds.

Table 1. Sample efficiency on Classic Control environments. Median steps to threshold (lower is better), with success rates in parentheses. SPAN achieves faster learning and higher success rates across all tasks.

Environment	Method	25%	50%	75%	95%	100%
CartPole	SPAN	36k (100%)	<b>73k (100%)</b>	<b>100k (95%)</b>	<b>145k (95%)</b>	<b>201k (95%)</b>
	MLP	<b>20k (95%)</b>	86k (95%)	201k (95%)	218k (90%)	300k (75%)
LunarLander	SPAN	<b>273k (100%)</b>	<b>283k (100%)</b>	<b>430k (95%)</b>	<b>560k (95%)</b>	<b>618k (90%)</b>
	MLP	348k (100%)	476k (100%)	621k (95%)	751k (75%)	810k (60%)
Acrobot	SPAN	<b>95k (100%)</b>	<b>105k (100%)</b>	<b>111k (95%)</b>	<b>130k (90%)</b>	<b>145k (90%)</b>
	MLP	175k (100%)	175k (70%)	198k (60%)	220k (60%)	228k (60%)

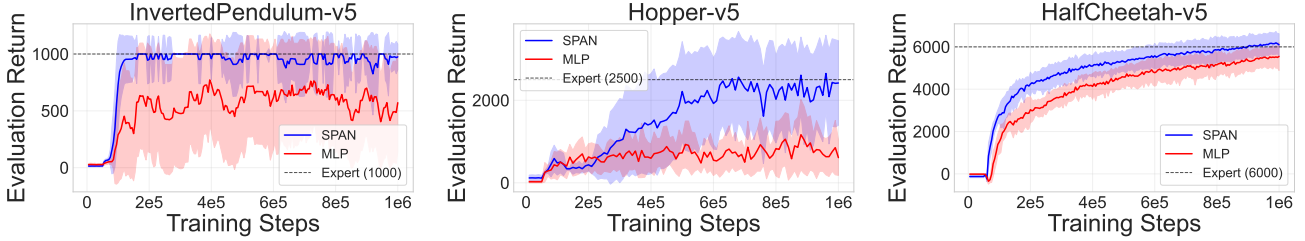


Figure 3. Learning curves for MuJoCo continuous control environments showing mean episodic return  $\pm$  one standard deviation across 20 random seeds.

Hopper is a locomotion task in which a planar one legged robot must learn to hop forward efficiently while maintaining balance. HalfCheetah models a planar bipedal agent with articulated joints that must learn to run forward at high speed.

Figure 3 reports learning curves showing mean episodic return with  $\pm$  one standard deviation across 20 random seeds. Table 2 reports sample efficiency results across multiple performance thresholds.

Hopper highlights SPAN’s advantage over MLP. At the 50% performance threshold, SPAN achieves a 90% success rate with a median solve time of 475k environment steps, while MLP reaches only 10% success at 715k steps. At higher thresholds (75% and above), MLP fails to achieve successful solutions across all seeds, whereas SPAN maintains success rates between 80% and 90%.

InvertedPendulum exhibits the most dramatic relative improvement. SPAN reaches the 75% performance thresh-

old in 100k steps, compared to 178k steps for MLP, corresponding to a 44% reduction in required interactions. Although both methods ultimately achieve perfect success rates, SPAN consistently converges approximately 2.2 $\times$  faster across all thresholds.

On HalfCheetah, both methods achieve strong final performance, but SPAN consistently improves sample efficiency. At the 50% threshold, SPAN solves the task in 120k steps compared to 193k steps for MLP (38% faster). This advantage increases at higher thresholds: 245k versus 485k steps at 75% (49% faster), and at the 95% threshold SPAN achieves a 90% success rate compared to 35% for MLP, with median solve times of 590k and 850k steps, respectively.

## 5.2. Offline Reinforcement Learning Results

To assess SPAN’s effectiveness beyond online learning, SPAN is also evaluated on offline RL using Implicit Q-Learning (IQL) (Kostrikov et al., 2021) on the D4RL (Fu

Table 2. Sample efficiency on MuJoCo environments. Median steps to threshold (lower is better), with success rates in parentheses. SPAN achieves faster learning and higher success rates across all tasks.

Environment	Method	25%	50%	75%	95%	100%
Hopper	SPAN	<b>310k (95%)</b>	<b>475k (90%)</b>	<b>510k (90%)</b>	<b>495k (80%)</b>	<b>495k (80%)</b>
	MLP	435k (90%)	715k (10%)	— (0%)	— (0%)	— (0%)
InvertedPendulum	SPAN	<b>95k (100%)</b>	<b>100k (100%)</b>	<b>100k (100%)</b>	<b>100k (100%)</b>	<b>100k (100%)</b>
	MLP	178k (100%)	178k (100%)	178k (100%)	178k (100%)	178k (100%)
HalfCheetah	SPAN	<b>75k (100%)</b>	<b>120k (100%)</b>	<b>245k (100%)</b>	<b>590k (90%)</b>	<b>698k (60%)</b>
	MLP	100k (100%)	193k (100%)	485k (100%)	850k (35%)	900k (10%)

et al., 2021) Adroit Hand Manipulation benchmark from Minari (Younis et al., 2024). Table 3 presents normalized performance scores across four dexterous manipulation tasks (Door, Hammer, Pen, Relocate) with three dataset qualities: Expert (near-optimal demonstrations), Cloned (behavioral cloning data), and Human (suboptimal human teleoperations). SPAN consistently outperforms MLP baselines on Expert datasets, achieving substantial improvements on challenging tasks: Door (8.0 vs 0.4, 20x improvement), Hammer (44.1 vs 19.3, 2.3x improvement), and Relocate (17.3 vs 5.2, 3.3x improvement). On Pen, both methods achieve strong expert-level performance (SPAN: 124.1, MLP: 119.6), with SPAN showing marginally higher scores. Performance on lower quality datasets (Cloned, Human) reveals more mixed results. SPAN maintains advantages on Pen across all dataset types (8.8 vs 6.7 on Cloned, 21.1 vs -10.0 on Human), suggesting robustness to demonstration quality. However, on Door, Hammer human datasets, MLP baselines show slight edges. This asymmetry reflects the interaction between SPAN’s smoothness bias and dataset characteristics: expert demonstrations exhibit smooth, consistent policies that align with B-spline approximation, while human datasets contain erratic behaviors and sharp transitions that challenge smooth function approximation. These results demonstrate SPAN’s advantages extend beyond online learning to offline RL, particularly when learning from high quality demonstrations. The dramatic improvements on expert datasets (2-20x on three of four tasks) suggest SPAN is especially valuable for imitation learning scenarios where smooth, expert level behaviors dominate the dataset.

### 5.3. Ablation Studies

To characterize the sensitivity of SPAN to its structural hyperparameters, grid searches are conducted across both discrete and continuous control environments. Three key architectural parameters: the tensor rank ( $M$ , corresponding to nmodes), the grid resolution ( $N$ , corresponding to nelems), and the polynomial degree of the B-splines ( $k$ ) are varied. Acrobot (discrete) and HalfCheetah (continuous) are presented here as a representative results, and full ablation results for all other environments are provided in Appendix C. Each panel shows the effect of varying a sin-

Table 3. Normalized Offline RL Performance on Minari Adroit (v2) Scores are normalized using standard D4RL reference constants. SPAN outperforms the MLP baseline on all Expert datasets.

Task	Dataset	SPAN (Ours)	MLP (Baseline)
Door	Expert	<b>8.0</b> $\pm$ 11.6	0.4 $\pm$ 0.0
	Cloned	<b>0.6</b> $\pm$ 0.1	<b>0.6</b> $\pm$ 0.1
	Human	0.5 $\pm$ 0.1	<b>1.2</b> $\pm$ 1.3
Hammer	Expert	<b>44.1</b> $\pm$ 38.3	19.3 $\pm$ 23.4
	Cloned	<b>0.3</b> $\pm$ 0.0	<b>0.3</b> $\pm$ 0.0
	Human	0.5 $\pm$ 0.3	<b>0.9</b> $\pm$ 0.6
Pen	Expert	<b>124.1</b> $\pm$ 19.8	119.6 $\pm$ 19.7
	Cloned	<b>8.8</b> $\pm$ 19.2	6.7 $\pm$ 13.3
	Human	<b>21.1</b> $\pm$ 31.8	-10.0 $\pm$ 6.1
Relocate	Expert	<b>17.3</b> $\pm$ 8.6	5.2 $\pm$ 3.0
	Cloned	<b>0.4</b> $\pm$ 0.1	<b>0.4</b> $\pm$ 0.0
	Human	<b>0.3</b> $\pm$ 0.0	<b>0.3</b> $\pm$ 0.0

gle architectural hyperparameter tensor rank ( $M$  / nmodes), grid resolution ( $N$  / nelems), and B-spline degree ( $k$ ) while keeping all other settings fixed. The distributions are shown as box plots over multiple independent training runs. In each box plot, the central line denotes the median final evaluation return, the box spans the interquartile range (25th-75th percentiles), and the whiskers indicate the full range of observed values.

Figure 4 illustrates the hyperparameter sensitivity for Acrobot. Performance remains remarkably stable across all configurations. Increasing the rank from  $M = 2$  to  $M = 10$  or resolution from  $N = 2$  to  $N = 5$  yields negligible changes in final reward. This suggests that for lower dimensional control tasks, the low rank of SPAN is sufficient to capture the optimal policy even at minimal capacity.

For the 17-dimensional HalfCheetah task, optimized SPAN implementation is used, which fixes the spline degree to quadratic ( $k = 2$ ) to focus the search space on rank and resolution. As shown in Figure 5, this environment exhibits a distinct scaling law. Unlike Acrobot, HalfCheetah benefits significantly from increased resolution, with returns improving consistently as grid density increases from  $N = 2$  to  $N = 8$ . Similarly, increasing tensor rank from  $M = 10$  to  $M = 20$  yields a positive trend in asymptotic performance.

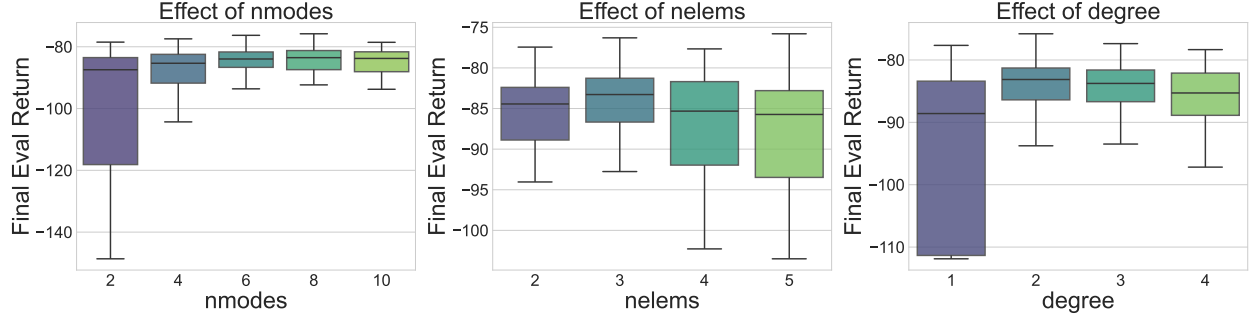


Figure 4. Ablation study on Acrobot-v1 showing performance vs. nmode, nelem, and degree.

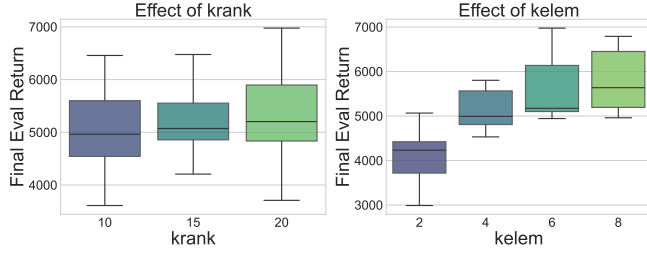


Figure 5. Ablation study on HalfCheetah-v5 showing performance vs. krank, kelem.

## 6. Discussion

This work demonstrates that SPAN is particularly effective in reinforcement learning regimes where samples, parameters, or training time are limited. Across both classic control, continuous control tasks, and high-dimensional adroit hand task SPAN consistently attains stronger policies with fewer environment interactions and remains effective under tight parameter budgets where standard MLPs often fail to learn. Moreover, SPAN exhibits improved anytime performance, producing useful policies early in training; an important property in practical deployments where training may be interrupted or computational budgets are uncertain.

These gains stem from architectural inductive biases that align with the structure of control problems. The use of B-spline bases introduces a local smoothness bias well suited to value functions and policies in physical systems, enabling efficient representation with fewer parameters than globally connected MLPs. In addition, smooth derivatives reduce optimization variance, leading to more stable learning across random seeds, while adaptive knot placement allows representational capacity to concentrate in critical regions of the state space. Unlike prior spline-based approaches relying on dense edge-wise constructions, SPAN’s low-rank tensor product structure achieves these benefits without incurring prohibitive computational overhead.

Despite these advantages, SPAN is not a universal replace-

ment for MLPs. When resources are abundant, MLPs remain appealing due to ubiquitous library support and well-understood scaling. Future work will study automated structure selection and extensions to discontinuous, multi-agent, and model-based settings where sample efficiency and anytime performance are critical.

## 7. Conclusion

Deploying reinforcement learning in resource-constrained environments, such as robotics with limited samples, edge devices with strict memory budgets, production systems with uncertain training durations, and for quick prototyping requires function approximators that learn efficiently. This work introduces SPAN, a novel function approximation paradigm for reinforcement learning that outperforms standard MLP baselines in extensive benchmarks across online and offline reinforcement learning. It achieves a 30-50% improvement in sample efficiency and 1.3-9 $\times$  higher success rates in online benchmarks and on offline expert datasets, SPAN outperforms the MLP baseline by an average factor of 6.7 $\times$ . These findings establish SPAN as a fundamentally more efficient representation for control. By offering parameter efficiency, reducing the number of environment interactions required for learning, SPAN reduces the computational demands of reinforcement learning, making it better suited for resource-constrained and energy-sensitive deployment scenarios. Overall, SPAN highlights the potential of structured function approximators for resource-constrained reinforcement learning and motivates further exploration of spline-based and tensorized architectures as first class alternatives to fully connected neural networks in control.

## Impact Statement

This work advances resource efficient reinforcement learning by introducing SPAN, a spline-based architecture that significantly reduces the number of environment interactions needed to learn high performance control policies by 30–50% compared to conventional approaches. These efficiency gains have significant practical implications across scientific and industrial domains. In healthcare, SPAN’s reduced sample requirements could accelerate clinical treatment optimization and drug dosing protocols, where patient interactions are costly or ethically constrained. In robotics, physical robot learning where each trial incurs mechanical wear, energy consumption, and supervision time can benefit from faster policy acquisition with fewer interactions. Domains requiring expensive simulations, such as climate modeling, materials science, and computational chemistry, can leverage SPAN to explore larger parameter spaces within fixed computational budgets. The architecture’s small memory footprint enables edge deployment in edge devices. Industries with uncertain training budgets or operational interruptions including manufacturing process optimization, autonomous vehicles can benefit from SPAN’s anytime performance guarantees, delivering functional policies even when training is prematurely halted.

While these methods could be applied to dual-use technologies, careful ethical oversight and rigorous safety validation remain essential. Practitioners are encouraged to consider both capabilities and limitations when deploying SPAN in real-world systems, particularly in safety-critical domains like healthcare, transportation, and infrastructure control. Reduced training variance and reliable convergence make SPAN suitable for applications requiring predictable behavior, but rigorous testing, safety validation, and ongoing monitoring remain essential. Future work should explicitly integrate fairness, safety, and societal impact considerations alongside efficiency metrics, ensuring that advances in sample-efficient reinforcement learning benefit society broadly.

## References

Ba, J. L., Kiros, J. R., and Hinton, G. E. Layer normalization, 2016. URL <https://arxiv.org/abs/1607.06450>.

Batley, R. T. and Saha, S. Khronos: a kernel-based neural architecture for rapid, resource-efficient scientific computation, 2025. URL <https://arxiv.org/abs/2505.13315>.

Batley, R. T. and Saha, S. *A Unified Generative-Predictive Framework for Deterministic Inverse Design*. 2026. doi: 10.2514/6.2026-0365. URL <https://arc.aiaa.org/doi/10.2514/6.2026-0365>.

Dulac-Arnold, G., Mankowitz, D., and Hester, T. Challenges of real-world reinforcement learning, 2019. URL <https://arxiv.org/abs/1904.12901>.

Fu, J., Kumar, A., Nachum, O., Tucker, G., and Levine, S. D4rl: Datasets for deep data-driven reinforcement learning, 2021. URL <https://arxiv.org/abs/2004.07219>.

Guo, H., Li, F., Li, J., and Liu, H. Kan v.s. mlp for offline reinforcement learning, 2024. URL <https://arxiv.org/abs/2409.09653>.

Haarnoja, T., Zhou, A., Abbeel, P., and Levine, S. Soft actor-critic: Off-policy maximum entropy deep reinforcement learning with a stochastic actor, 2018. URL <https://arxiv.org/abs/1801.01290>.

Haarnoja, T., Zhou, A., Hartikainen, K., Tucker, G., Ha, S., Tan, J., Kumar, V., Zhu, H., Gupta, A., Abbeel, P., and Levine, S. Soft actor-critic algorithms and applications, 2019. URL <https://arxiv.org/abs/1812.05905>.

Han, S., Mao, H., and Dally, W. J. Deep compression: Compressing deep neural networks with pruning, trained quantization and huffman coding, 2016. URL <https://arxiv.org/abs/1510.00149>.

He, K., Zhang, X., Ren, S., and Sun, J. Deep residual learning for image recognition, 2015. URL <https://arxiv.org/abs/1512.03385>.

Henderson, P., Islam, R., Bachman, P., Pineau, J., Precup, D., and Meger, D. Deep reinforcement learning that matters, 2019. URL <https://arxiv.org/abs/1709.06560>.

Hendrycks, D. and Gimpel, K. Gaussian error linear units (gelus), 2023. URL <https://arxiv.org/abs/1606.08415>.

Hinton, G., Vinyals, O., and Dean, J. Distilling the knowledge in a neural network, 2015. URL <https://arxiv.org/abs/1503.02531>.

Hornik, K. et al. Multilayer feedforward networks are universal approximators. *Neural Networks*, 2(5):359–366, 1989.

Jacob, B., Kligys, S., Chen, B., Zhu, M., Tang, M., Howard, A., Adam, H., and Kalenichenko, D. Quantization and training of neural networks for efficient integer-arithmetic-only inference, 2017. URL <https://arxiv.org/abs/1712.05877>.

Kahn, G. et al. Plato: Policy learning using adaptive trajectory optimization, 2017.

Kakade, S. *On the Sample Complexity of Reinforcement Learning*. PhD thesis, University College London, 2003.

Kalashnikov, D. et al. Qt-opt: Scalable deep reinforcement learning for vision-based robotic manipulation, 2018.

Kich, V. A., Bottega, J. A., Steinmetz, R., Grando, R. B., Yorozu, A., and Ohya, A. Kolmogorov-arnold network for online reinforcement learning, 2024. URL <https://arxiv.org/abs/2408.04841>.

Kostrikov, I., Nair, A., and Levine, S. Offline reinforcement learning with implicit q-learning, 2021. URL <https://arxiv.org/abs/2110.06169>.

Levine, S. et al. End-to-end training of deep visuomotor policies. *Journal of Machine Learning Research*, 17(39):1–40, 2016.

Li, Y. et al. Edge ai: On-demand accelerating deep neural network inference via edge computing. *IEEE Transactions on Computers*, 2020.

Lillicrap, T. P., Hunt, J. J., Pritzel, A., Heess, N., Erez, T., Tassa, Y., Silver, D., and Wierstra, D. Continuous control with deep reinforcement learning, 2019. URL <https://arxiv.org/abs/1509.02971>.

Liu, Z., Wang, Y., Vaidya, S., Ruehle, F., Halverson, J., Soljačić, M., Hou, T. Y., and Tegmark, M. Kan: Kolmogorov-arnold networks, 2025. URL <https://arxiv.org/abs/2404.19756>.

Mao, H. et al. Resource management with deep reinforcement learning. In *ACM HotNets*, 2016.

Mnih, V. et al. Human-level control through deep reinforcement learning. *Nature*, 518(7540):529–533, 2015.

Mostakim, R., Batley, R. T., and Saha, S. A framework toward knowledge transfer across heterogeneous and sparse datasets for fatigue life estimation of additively manufactured alloys. *International Journal of Fatigue*, 202:109185, 2025. ISSN 0142-1123. doi: <https://doi.org/10.1016/j.ijfatigue.2025.109185>. URL <https://www.sciencedirect.com/science/article/pii/S0142112325003822>.

Novikov, A., Podoprikin, D., Osokin, A., and Vetrov, D. Tensorizing neural networks, 2015. URL <https://arxiv.org/abs/1509.06569>.

Park, C., Saha, S., Guo, J., Zhang, H., Xie, X., Bessa, M. A., Qian, D., Chen, W., Wanger, G. J., Cao, J., Hughes, T. J. R., and Liu, W. K. Unifying machine learning and interpolation theory via interpolating neural networks. *Nature Communications*, 16(1):8753, 2025. ISSN 2041-1723. doi: 10.1038/s41467-025-63790-8. URL <https://doi.org/10.1038/s41467-025-63790-8>.

Ramachandran, P., Zoph, B., and Le, Q. V. Searching for activation functions, 2017. URL <https://arxiv.org/abs/1710.05941>.

Sainath, T. N., Kingsbury, B., Sindhwani, V., Arisoy, E., and Ramabhadran, B. Low-rank matrix factorization for deep neural network training with high-dimensional output targets. In *2013 IEEE international conference on acoustics, speech and signal processing*, pp. 6655–6659, 2013.

Sarker, A., Batley, R. T., Sarojini, D., and Saha, S. A Kernel-based Resource-efficient Neural Surrogate for Multi-fidelity Prediction of Aerodynamic Field. 2026. doi: 10.2514/6.2026-0043. URL <https://arc.aiaa.org/doi/abs/10.2514/6.2026-0043>.

Schulman, J., Wolski, F., Dhariwal, P., Radford, A., and Klimov, O. Proximal policy optimization algorithms, 2017. URL <https://arxiv.org/abs/1707.06347>.

Schulman, J., Moritz, P., Levine, S., Jordan, M., and Abbeel, P. High-dimensional continuous control using generalized advantage estimation, 2018. URL <https://arxiv.org/abs/1506.02438>.

Silver, D. et al. Mastering the game of go without human knowledge. *Nature*, 550:354–359, 2017.

Sutton, R. S. and Barto, A. G. *Reinforcement Learning: An Introduction*. MIT Press, 2nd edition, 2018.

Sutton, R. S., McAllester, D., Singh, S., and Mansour, Y. Policy gradient methods for reinforcement learning with function approximation. In *Advances in Neural Information Processing Systems*, volume 12, 1999.

Tai, L. et al. Virtual-to-real deep reinforcement learning: Continuous control of mobile robots for mapless navigation. *IEEE/RSJ IROS*, 2017.

Towers, M., Kwiatkowski, A., Terry, J., Balis, J. U., De Cola, G., Deleu, T., Goulão, M., Kallinteris, A., Krimmel, M., KG, A., et al. Gymnasium: A standard interface for reinforcement learning environments. *arXiv preprint arXiv:2407.17032*, 2024.

Younis, O. G., Perez-Vicente, R., Balis, J. U., Dudley, W., Davey, A., and Terry, J. K. Minari, September 2024. URL <https://doi.org/10.5281/zenodo.13767625>.

Zilberstein, S. Using anytime algorithms in intelligent systems. *AI Magazine*, 17(3):73–83, 1996.

## A. Anytime Performance

This section presents comprehensive anytime performance results across all environments. The agent performance is evaluated at five checkpoints during training: 10% (100k), 25% (250k), 50% (500k), 75% (750k), and 100% (1M) of the total training budget steps. For each checkpoint, mean score across 20 seeds, standard deviation are reported.

Table 4 presents anytime performance for CartPole, LunarLander, and Acrobot. SPAN demonstrates consistent advantages across all checkpoints, with particularly pronounced benefits during early training phases when sample efficiency matters most.

Table 4. Anytime performance on Classic Control environments. Mean score  $\pm$  std across 20 seeds at each training checkpoint.

Environment	Method	10%	25%	50%	75%	95%	100%
CartPole	SPAN	247 $\pm$ 141	<b>359<math>\pm</math>153</b>	<b>482<math>\pm</math>71</b>	<b>488<math>\pm</math>54</b>	<b>490<math>\pm</math>45</b>	<b>491<math>\pm</math>38</b>
	MLP	247 $\pm$ 134	221 $\pm$ 125	429 $\pm$ 123	449 $\pm$ 128	461 $\pm$ 113	464 $\pm$ 112
LunarLander	SPAN	<b>-529<math>\pm</math>565</b>	<b>26<math>\pm</math>116</b>	<b>160<math>\pm</math>66</b>	<b>199<math>\pm</math>40</b>	<b>204<math>\pm</math>48</b>	<b>218<math>\pm</math>55</b>
	MLP	-785 $\pm$ 711	-14 $\pm$ 65	108 $\pm$ 52	178 $\pm$ 39	196 $\pm$ 33	195 $\pm$ 39
Acrobot	SPAN	<b>-445<math>\pm</math>105</b>	<b>-223<math>\pm</math>178</b>	<b>-134<math>\pm</math>127</b>	<b>-112<math>\pm</math>94</b>	<b>-108<math>\pm</math>93</b>	<b>-104<math>\pm</math>93</b>
	MLP	-468 $\pm$ 98	-430 $\pm$ 145	-302 $\pm$ 206	-250 $\pm$ 209	-222 $\pm$ 193	-216 $\pm$ 193

On **CartPole**, SPAN shows stable learning from early checkpoints, while MLPs exhibit a notable performance dip at 25% (221 $\pm$ 125) before recovering. By 50% of training, SPAN achieves 482 $\pm$ 71 return compared to MLPs' 429 $\pm$ 123, demonstrating both higher performance and substantially lower variance (71 vs 123 standard deviation). This stability advantage persists through final convergence, with SPAN maintaining tighter variance bounds throughout training.

**LunarLander** reveals SPAN's most dramatic early learning advantages. At 25% of training budget, SPAN achieves positive returns (26 $\pm$ 116) while MLPs remain slightly negative (-14 $\pm$ 65). By 50% checkpoint, SPAN reaches 160 $\pm$ 66 already 73% of its final performance compared to MLPs at 108 $\pm$ 52 (55% of final). This 40% sample efficiency improvement at mid-training translates directly to reduced costs in sample expensive domains. Notably, SPAN continues improving through final convergence (218 $\pm$ 55) while MLP performance plateaus around 75% (178 $\pm$ 39  $\rightarrow$  195 $\pm$ 39).

For **Acrobot**, SPAN demonstrates superior performance at every checkpoint with remarkably consistent improvement. The 25% checkpoint comparison is particularly striking: SPAN achieves -223 $\pm$ 178 versus MLPs at -430 $\pm$ 145, a 63% reduction in policy quality gap. Even at 10%, SPAN shows modestly better mean performance with slightly higher variance, suggesting more exploratory but ultimately more successful learning dynamics. Final convergence maintains SPAN's advantage: -104 $\pm$ 93 versus -216 $\pm$ 193, representing both better final performance and 52% variance reduction.

Table 5 presents anytime performance on Hopper, InvertedPendulum, and HalfCheetah. Across all MuJoCo tasks substantially more complex than classic control SPAN demonstrates faster learning, more stable convergence, and dramatically reduced training variance.

Table 5. Anytime performance on MuJoCo environments. Mean score  $\pm$  std across 20 seeds at each training checkpoint.

Environment	Method	10%	25%	50%	75%	95%	100%
Hopper	SPAN	<b>480<math>\pm</math>293</b>	<b>728<math>\pm</math>633</b>	<b>2213<math>\pm</math>1208</b>	<b>2371<math>\pm</math>1117</b>	<b>2366<math>\pm</math>1120</b>	<b>2647<math>\pm</math>971</b>
	MLP	407 $\pm$ 335	504 $\pm$ 225	726 $\pm$ 386	925 $\pm$ 643	693 $\pm$ 414	611 $\pm$ 431
InvertedPendulum	SPAN	<b>728<math>\pm</math>386</b>	<b>953<math>\pm</math>212</b>	<b>926<math>\pm</math>227</b>	<b>1000<math>\pm</math>0</b>	<b>1000<math>\pm</math>0</b>	<b>975<math>\pm</math>113</b>
	MLP	289 $\pm$ 422	431 $\pm$ 478	619 $\pm$ 479	646 $\pm$ 449	454 $\pm$ 427	571 $\pm$ 432
HalfCheetah	SPAN	<b>2808<math>\pm</math>380</b>	<b>4463<math>\pm</math>543</b>	<b>5308<math>\pm</math>458</b>	<b>5795<math>\pm</math>566</b>	<b>6099<math>\pm</math>542</b>	<b>6099<math>\pm</math>527</b>
	MLP	1518 $\pm$ 584	3229 $\pm$ 437	4576 $\pm$ 506	5118 $\pm$ 596	5504 $\pm$ 468	5544 $\pm$ 659

**Hopper** exemplifies SPAN's advantages on complex continuous control. From 10% onward, SPAN maintains performance advantages that compound through training. The 50% checkpoint reveals the critical difference: SPAN achieves 2213 $\pm$ 1208 (84% of final performance) while MLPs reach only 726 $\pm$ 386 (119% of final, actually exceeding final performance,

indicating training instability). MLP performance degrades after 50%, dropping from  $925\pm643$  at 75% to  $611\pm431$  at convergence, suggesting policy collapse or catastrophic forgetting. In contrast, SPAN shows monotonic improvement with final performance of  $2647\pm971$  a  $4.3\times$  advantage over MLPs'  $611\pm431$ . For practitioners, this means SPAN delivers usable policies at every checkpoint while MLPs risk complete failure.

**InvertedPendulum** demonstrates SPAN's reliability through unprecedented stability. At 25% budget, SPAN achieves  $953\pm212$  already 95% of optimal (expert baseline: 1000) while MLPs reach only  $431\pm478$  (43% of optimal). By 75%, SPAN achieves perfect performance with zero variance ( $1000\pm0$ ), maintaining this through 95% before minor degradation at final checkpoint ( $975\pm113$ ). MLPs never achieve consistent convergence, with final performance of  $571\pm432$  and persistent high variance indicating roughly half of training runs fail completely. This reliability difference is critical for production deployments where consistent performance across random seeds is essential.

**HalfCheetah** shows SPAN's sample efficiency advantages on high-dimensional continuous control. At just 10% of training (100k steps), SPAN achieves  $2808\pm380$  versus MLPs'  $1518\pm584$  an 85% performance advantage (46% vs 27% of respective final performance). This gap persists through mid-training: at 50%, SPAN reaches  $5308\pm458$  (87% of final) compared to MLPs'  $4576\pm506$  (83% of final). While both methods eventually converge to respectable performance (SPAN:  $6099\pm527$ , MLP:  $5544\pm659$ ), SPAN's 10% advantage and consistently lower variance demonstrate its practical value for resource-constrained training scenarios.

### A.1. Key Insights

These anytime performance results reveal three critical patterns. First, SPAN provides substantially better policies when training terminates early: at 25% budget, SPAN shows 24-71% better performance across environments, translating to usable controllers versus non functional policies. Second, SPAN exhibits dramatically reduced variance, particularly visible in InvertedPendulum ( $1000\pm0$  vs  $646\pm449$  at 75%) and Acrobot ( $-104\pm93$  vs  $-216\pm193$  final), indicating reliable convergence across random seeds. Third, MLP training on complex task (Hopper) shows instability performance degradation after mid-training or high variance indicating frequent failures while SPAN maintains monotonic or stable improvement. For practitioners facing uncertain training budgets, hardware constraints, or requiring reliable convergence, these anytime performance characteristics make SPAN substantially more practical than standard MLPs despite comparable final performance in best case scenarios.

## B. Training Details and Hyperparameters

This section provides complete hyperparameter configurations for reproducibility. All experiments use 20 random seeds with matched parameter budgets between SPAN and MLP baselines.

Table 6 summarizes total steps and number of seeds for training and ablation studies for each environment.

*Table 6.* Training and ablation settings. Steps and seeds refer to independent training runs.

Domain	Environment	Train		Ablation	
		Steps	Seeds	Steps	Seeds
Classic Control	CartPole-v1	500k	20	300k	5
Classic Control	Acrobot-v1	500k	20	300k	5
Box2D	LunarLander-v3	1M	20	1M	5
MuJoCo	InvertedPendulum-v5	1M	20	400k	5
	Hopper-v5	1M	20	400k	5
	HalfCheetah-v5	1M	20	400k	5

Table 7 shows hyperparameters across environments within each domain. Classic Control uses PPO while MuJoCo uses SAC. And for offline learning IQL algorithm is used.

The number of parameters for SPAN and MLP architectures in online reinforcement learning is summarized in Table 8, with Table 9 presenting the values for offline reinforcement learning.

Table 7. Common training hyperparameters by learning paradigm

Parameter	Online RL		Offline RL
	Classic Control (PPO)	MuJoCo (SAC)	IQL
Total timesteps / iterations	$5 \times 10^5$	$1 \times 10^6$	20,000
Batch size	1024 (rollout)	128	256
Mini-batch size	64	—	—
Update epochs	4	1	—
Discount factor ( $\gamma$ )	0.99	0.99	0.99
GAE $\lambda$	0.95	—	—
Learning rate	$3 \times 10^{-4}$	$3 \times 10^{-4}$	$3 \times 10^{-4}$
Value loss coefficient ( $c_v$ )	0.5	—	—
Clip coefficient	0.2	—	—
Max grad norm	0.5	10.0	—
Replay buffer size	—	$1 \times 10^6$	Offline dataset
Random exploration steps	—	50,000	—
Soft update ( $\tau$ )	—	0.005	0.005
Target entropy scale / temperature	—	1.0	3.0
Expectile ( $\tau_{\text{exp}}$ )	—	—	0.7
Evaluation interval	5,000 steps	5,000 steps	—
Evaluation episodes	30	30	100
Number of seeds	20	20	5

Table 8. Environment specific parameters

Environment	MLP Actor	MLP Critic	nmodes	nelems	degree	MLP Params	SPAN Params
<i>Classic Control</i>							
CartPole-v1	(4, 3)	(4, 4)	1	2	1	88	86
Acrobot-v1	(13, 13)	(13, 13)	6	2	1	602	472
LunarLander-v3	(18, 17)	(20, 19)	11	2	1	1156	1084
<i>MuJoCo</i>							
InvertedPendulum-v5	(6, 5)	(6, 7)	2	2	2	256	260
Hopper-v5	(25, 24)	(29, 29)	10	8	2	3744	3799
HalfCheetah-v5	(21, 21)	(28, 28)	10	4	2	4130	4147

Table 9. Environment specific parameters

Environment	MLP Actor	MLP Critic	MLP Value	nmodes	nelems	degree	MLP Params	SPAN Params
<i>Adroit - Door</i>								
Expert	(36,36)	(64,64)	(45,45)	15	4	2	17337	17449
Cloned	(36,36)	(64,64)	(45,45)	15	4	2	17337	17449
Human	(36,36)	(64,64)	(45,45)	15	4	2	17337	17449
<i>Adroit - Hammer</i>								
Expert	(41,41)	(68,68)	(50,50)	15	4	2	20509	20448
Cloned	(41,41)	(68,68)	(50,50)	15	4	2	20509	20448
Human	(41,41)	(68,68)	(50,50)	15	4	2	20509	20448
<i>Adroit - Pen</i>								
Expert	(41,41)	(66,66)	(50,50)	15	4	2	19634	19469
Cloned	(41,41)	(66,66)	(50,50)	15	4	2	19634	19469
Human	(41,41)	(66,66)	(50,50)	15	4	2	19634	19469
<i>Adroit - Relocate</i>								
Expert	(35,35)	(66,66)	(45,45)	15	4	2	17845	17909
Cloned	(35,35)	(66,66)	(45,45)	15	4	2	17845	17909
Human	(35,35)	(66,66)	(45,45)	15	4	2	17845	17909

## C. Complete Ablation Studies

Systematic ablation studies are conducted across CartPole, InvertedPendulum, LunarLander, and Hopper to understand the impact of SPAN’s architectural hyperparameters: *nmodes* (number of tensor product modes), *nelems* (number of B-spline elements per dimension), and *degree* (polynomial degree of B-splines).

**CartPole-v1** demonstrates remarkable stability across all hyperparameter ranges. The environment maintains optimal return ( $\sim 500$ ) across  $n\text{modes} \in [1, 9]$ ,  $n\text{elems} \in [2, 5]$ , and  $\text{degree} \in [1, 4]$ , with flat response curves indicating complete saturation at minimal capacity. This suggests that even the smallest SPAN configurations provide sufficient representational power for simple control tasks.

**InvertedPendulum-v5** reveals critical threshold effects in architectural capacity. Configurations with  $n\text{modes}=2$  and  $n\text{elems}=2$  achieve near-optimal performance ( $\sim 1000$  return), while minimal settings ( $n\text{modes}=1$ ,  $n\text{elems}=1$ ,  $\text{degree}=1$ ) cause catastrophic failure with returns dropping to 400-600. Notably, once the minimum complexity threshold is exceeded, performance saturates immediately with no additional benefit from increased capacity, highlighting a sharp phase transition in model expressiveness.

**LunarLander-v2** exhibits more nuanced sensitivity patterns. Performance improves progressively with *nmodes*, increasing from  $\sim 150$  return at *nmodes*=5 to  $\sim 200$  at *nmodes*=13, indicating that this moderately complex task benefits from additional representational modes. The *nelems* parameter displays a clear threshold: *nelems*=1 yields poor performance ( $\sim 100$  return) while *nelems*  $\geq 2$  achieves stable performance ( $\sim 200$  return). The *degree* parameter remains relatively invariant across [1,3], suggesting polynomial order has minimal impact once other capacity requirements are satisfied.

**Hopper-v5**, as one of the most complex MuJoCo environments in our evaluation, demonstrates substantial capacity requirements with high performance variance. Increasing *krank* (equivalent to *nmodes*) from 6 to 10 shows clear improvements in median performance alongside marked reduction in failure cases. The *kelem* parameter (equivalent to *nelems*) exhibits particularly strong effects: *kelem*=4 produces highly variable outcomes (500-2500 return range), while *kelem*=8 achieves both superior and more consistent results (median  $\sim 3000$  return with substantially tighter distribution), underscoring the importance of adequate capacity for complex continuous control.

**Summary.** Ablation studies reveal a clear pattern: simple tasks (CartPole, InvertedPendulum) are insensitive to hyperparameter choices once minimal capacity thresholds are met, while complex tasks (LunarLander, Hopper) benefit from higher capacity configurations ( $n\text{modes} \geq 10$ ,  $n\text{elems} \geq 6$  for MuJoCo). Critically, once capacity thresholds are exceeded, performance stabilizes across wide hyperparameter ranges, demonstrating SPAN’s practical robustness and eliminating the need for extensive environment-specific tuning.

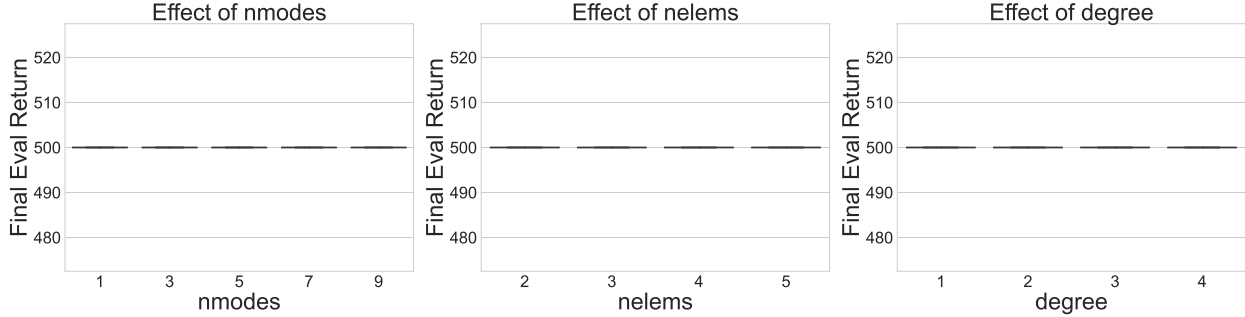


Figure 6. Ablation study on CartPole-v1 showing performance vs. *nmodes*, *nelems*, and *degree*.

## D. Hardware Specification

All experiments were conducted on a laptop computer with the following specifications:

- **Processor:** Intel(R) Core(TM) i9-14900HX @ 2.20 GHz
- **RAM:** 32.0 GB (31.7 GB usable) @ 5600 MT/s

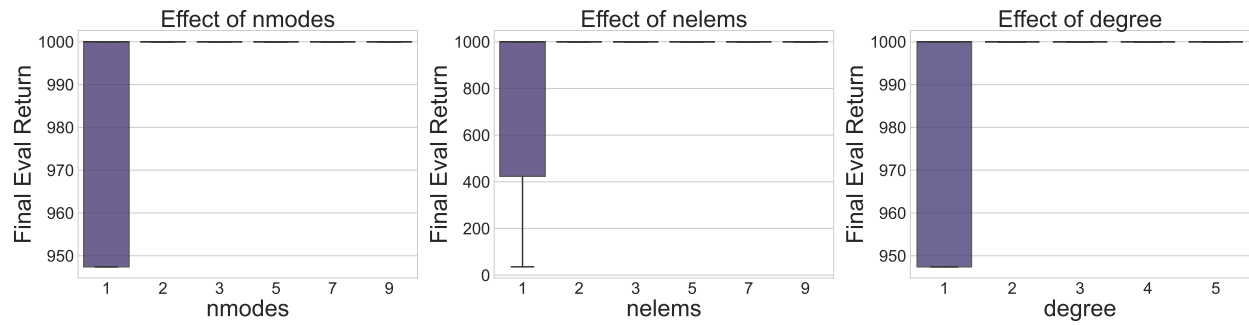


Figure 7. Ablation study on InvertedPendulum-v5 showing performance vs. nmodes, nelems, and degree.

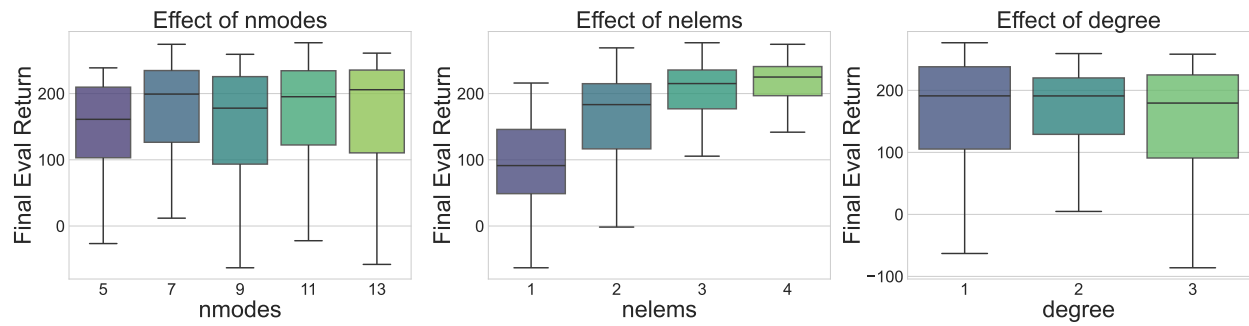


Figure 8. Ablation study on LunarLander-v3 showing performance vs. nmodes, nelems, and degree.

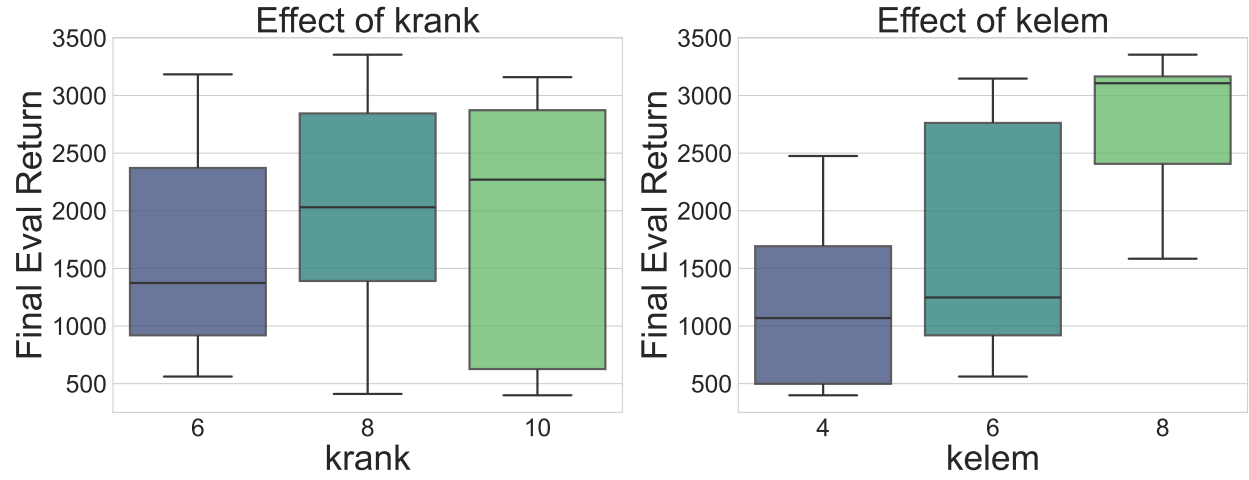


Figure 9. Ablation study Hopper showing performance vs. krank and kelem

- **Graphics:** NVIDIA GeForce RTX 5060 (8 GB VRAM)
- **Storage:** 954 GB SSD
- **Operating System:** Windows 11, 64-bit, x64-based processor